

## Article

# Investigation of Thermoplastic Polyurethane Finger Cushion with Magnetorheological Fluid for Soft-Rigid Gripper

Marcin Białek <sup>1,\*</sup> , Cezary Jędrzycka <sup>2</sup>  and Andrzej Milecki <sup>1</sup> 

<sup>1</sup> Division of Mechatronic Devices, Poznan University of Technology, 60-965 Poznan, Poland; andrzej.milecki@put.poznan.pl

<sup>2</sup> Division of Mechatronics and Electrical Machines, Poznan University of Technology, 60-965 Poznan, Poland; cezary.jedryczka@put.poznan.pl

\* Correspondence: marcin.bialek@put.poznan.pl

**Abstract:** This paper presents a study of penetrating a pin into a magnetorheological fluid (MR) cushion focused on the force measurement. The research is supported by detailed finite element analysis (FEA) of the magnetic field distributions in several magnetic field exciters applied to control rheological properties of the MR inside the cushion. The cushion is a part of the finger pad of the jaw soft-rigid gripper and was made of thermoplastic polyurethane (TPU) using 3D printing technology. For the pin-penetrating setup, the use of a holding electromagnet and a magnetic holder were considered and verified by simulation as well as experiment. In further simulation studies, two design solutions using permanent magnets as the source of the magnetic field in the cushion volume to control MR fluid viscosity were considered. The primary aim of the study was to analyze the potential of using an MR fluid in a cushion pad and to investigate the potential for changing its viscosity using different magnetic field sources. The analysis included magnetic field simulations and tests of pin penetration in the cushion as an imitation of object grasping. Thus, an innovative application of 3D printing and TPU to work with MR fluid is proposed.

**Keywords:** magnetorheological (MR) fluid; finite element analysis (FEA); soft-rigid gripper; thermoplastic polyurethane (TPU); 3D printing; mechanical engineering



**Citation:** Białek, M.; Jędrzycka, C.; Milecki, A. Investigation of Thermoplastic Polyurethane Finger Cushion with Magnetorheological Fluid for Soft-Rigid Gripper. *Energies* **2021**, *14*, 6541. <https://doi.org/10.3390/en14206541>

Academic Editors: Davide Astolfi and Anouar Belahcen

Received: 27 August 2021

Accepted: 9 October 2021

Published: 12 October 2021

**Publisher's Note:** MDPI stays neutral with regard to jurisdictional claims in published maps and institutional affiliations.



**Copyright:** © 2021 by the authors. Licensee MDPI, Basel, Switzerland. This article is an open access article distributed under the terms and conditions of the Creative Commons Attribution (CC BY) license (<https://creativecommons.org/licenses/by/4.0/>).

## 1. Introduction

Interest in soft grippers continues to attract the attention of researchers [1], as does the application of magnetorheology in robotic grippers [2]. Nowadays, robotic grippers constitute a very extensive group of devices intended for the manipulation of objects, with soft grippers leading the way. They are also found in various forms, such as a single tentacle [3] or a three-fingered hand made of reinforced silicone [4]. Soft grippers are inspired by octopuses and their flexible tentacles, which have dual capabilities of pushing-based locomotion and grasping by wrapping around objects [5]. The main goals of soft gripping devices are precision and force exertion, but they feature a large number of degrees of freedom and structural compliance [6]. Their potential is continuously developed by introducing sleeves that provide a uniform reinforcement to reduce local stresses and strains [7] or by adding a rigid component to its structure [8]. In other soft-rigid solutions, the soft actuator may be located outside the rigid jaws, but it will determinate the gripping state of the gripper using a noncontact sensing method [9]. These approaches reduce the main disadvantage of soft grippers, i.e., the limited ability to handle higher loads. Due to the level of complexity of soft gripper components, conventional manufacturing methods are being outdated. For this purpose, shape deposition manufacturing (SDM) and smart composite microstructures (SCM) methods are used to enable the molding of complex bodies, actuators, and expandable electronics for soft robots [10]. Rigid components can also be replaced by flexible composites, e.g., wax-coated foams made of polyurethane and 3D-printed meshes. They allow great variety in volume, form, and modulus within

an easily achievable temperature range, as well as firm self-healing properties [11]. In addition to the use of this type of material, there are flexible structures, which find their main application in medical procedure applications [12,13]. An interesting proposition worthy of attention is the jamming gripper. It is basically an elastic bladder filled with a granular material or fluid that adapts to the shape of the object being grabbed, and while maintaining this state, the gripper is capable of holding the item. In the case of granular material, it is necessary to extract air from the cushion after the elastic bladder has been dented [14]. In turn, the use of MR fluids requires the insertion of a magnetic field source into the gripper design, for example, in the form of an electromagnet [15] or an electromagnet with an adjustable magnetic core [16,17]. A solution using an electromagnet in a bunch and a magnet at the bottom of the bag filled with water in a water gripper design has also been acknowledged [18].

Grippers of rigid construction, on the other hand, can be equipped with fingertips on the jaws that allow for additional adaptation to the surface of the gripping element while maintaining the properties of the rigid construction. Tests of several such solutions have already been presented. The first one is the use of a rubber bag filled with gel and equipped in silicone layer [19]. Such a solution allows to grip both delicate and heavy elements of high rigidity. In this case, the gel is an intermediate layer between the rubber bag and the silicone sphere. At the approach of the jaw with the cushion to the gripped object, the gel, by its incompressibility, allows to grip with low stiffness, then the cushion adapts to the shape, and the contact stiffness increases. According to the authors, the fingertips exert a uniform contact force at low maximum pressure. Fingertips can be filled with viscoelastic fluid [20]. In order to separate the rigid jaws from the object and better match their surface to its shape, rubber pockets filled with air can be used [21]. In this solution, the authors presented a two-jaw parallel gripper design in which pockets of different shapes were placed on the jaws and filled with air, forming soft cushions. During the feasibility tests, they observed slight opening of the side plates, especially when pressure is exerted on the rubber side pockets, which is caused by the width and flexibility of the side panels (jaws). Such cushions can also be filled with MR fluid to create a miniaturized solution similar to the jamming gripper [22]. In this case, the source of the magnetic field is a permanent magnet pushed against the pad using a mechanism based on a spring in a holder moving on a motor-driven screw through a belt transmission. The authors used hydrogenated nitrile butadiene rubber (HNBR) embedded on an iron yoke and secured with a clamp on the elastic bladder. The range of motion of the magnet relative to the base of the pad allows for simultaneous introduction and removal of a magnetic field within the pad. Tests included attempts to grip objects of various shapes and to measure gripping force with and without magnetic field. It is also worth noting the benefits of inserting pads on the jaws. In addition to matching the geometry of the gripped object, they also influence the increase of contact area and frictional behavior [23]. The authors note the consideration of curvature and thickness in pad design and indicate that the best frictional, shear strength, and holding force at low loads is exhibited by the cubic finger pad. It is followed by the sphere geometry, which was chosen for the tests presented in this paper because of the distributions of the applied magnetic field sources. The previously mentioned parameters also allow for within-hand pose manipulation [24], i.e., performing sliding, gripping, and rolling moves of the object. The pads can furthermore provide information on object handling by equipping them with force/tactile sensors [25]. This makes it possible to enrich the gripper control system with coupling and gripping information, especially when considering the slipping control algorithm. In addition, the possibility of using feedback loops to control grippers [26] and entire manipulators [27] must be also taken into account. There are also MR sponge cell solutions. These are based on soaking a sponge in MR liquid and encapsulating it in a cling film. This allows the MR sponge to deform while retaining its flexibility and ability to return to its original form and thus be controlled by an external magnetic field source [28]. A derivative of MR liquid-based solutions are grippers using magnetorheological elastomers (MREs), or smart composites based on carbonyl-iron

particles in a silicone rubber. These can be used, for example, to make gripper jaws that adapt to the shape of the object being gripped. In this case, the properties and behavior of jaws made from MREs are also influenced by the percentage of carbonyl-iron particles [29]. In particular, the article [30] provided inspiration for this research.

The main objective of this research was to analyze the further potential of using a magnetorheological fluid in a jaw gripper cushion (Figures 1 and 2) and to scope out ways to change its viscosity using different magnetic field sources. The goal was to include finite element analysis (FEA) and preliminary investigations of force acting on the pin during penetration in the pad, imitating real contact conditions with the gripped object. At the same time, a novel solution to fabricate the cushion using 3D printing from thermoplastic polyurethane (TPU) was proposed. They are intended to form the finger pads of the gripper jaws (Figure 1a). To control the elasticity of the finger pads, the spring-magnet mechanism (schematically illustrated in Figure 1c) is proposed in the study.

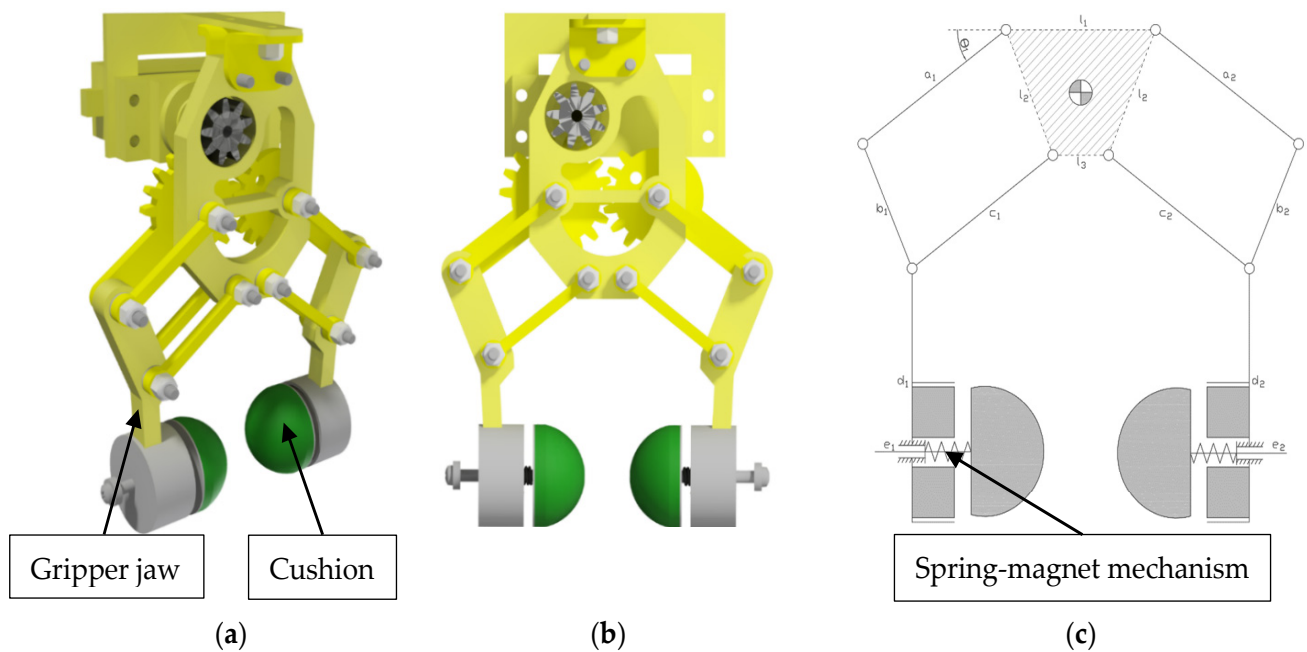


**Figure 1.** Gripper with thermoplastic polyurethane cushion-finger pads filled with MR fluid; (a) isometric view, (b) front view, (c) gripper kinematic schema.

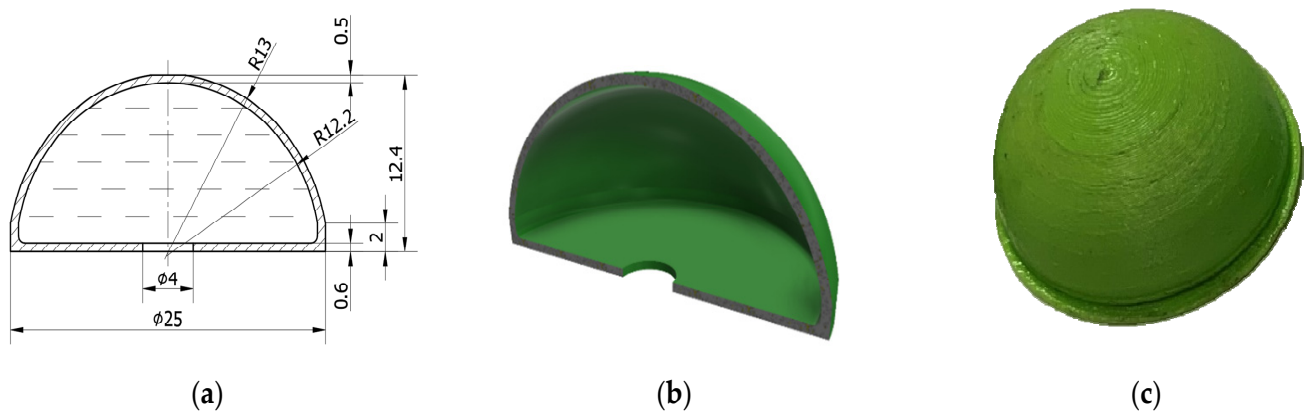


**Figure 2.** MR fluid cushion—a container for magnetorheological fluid; (a) cushion geometry, (b) cushion cross-section model, (c) cushion printed from TPU.

## 2. Materials and Methods

### 2.1. Cushion Structure

The initial idea was to create the cushion of flexible Fiberflex 30D filament using fused deposition modeling. This is a thermoplastic polyester elastomer with a Shore 30D hardness. Although the first prints were very promising, even short-term compression tests of the cushion showed its inability to maintain a seal. The thin walls determined that the print retained its flexibility, but consequently led to delamination of the dome. Therefore, an attempt was made to secure the liquid by introducing it into a latex balloon and securing it with a dome made of the previously mentioned flexible print. As the experiments showed, in the long term, the latex reacts with the liquid causing the oily part to precipitate out. As a result, after a week, the outer part of the balloon was oily from the oil, and a thick deposit of ferromagnetic particles remained in the balloon as a result of MR liquid segregation.

Further experiments have focused on the use of TPU because of its properties similar to flexible rubber. This material is also 3D printable. The printing tests conducted made it possible to obtain a monolithic, leak-proof cushion. In addition, long-term tests have shown that the MR fluid does not react with it even after several months of being inserted inside the cushion and sealed. The TPU cushion withstands repeated squeezing tests, showing tightness and resistance to wearing out. The geometry of the cushion is shown in Figure 2 and is based on a hemisphere with a diameter of 25 mm. The wall thickness varies between 0.5–0.6 mm. The basic parameters of FDM printing and TPU material are summarized in Tables 1 and 2. The cushion is filled with MR fluid by inserting a syringe through the hole at the base, filling the assumed volume and gluing a TPU disc of 25 mm diameter and 0.4 mm thickness with cyano-acrylic glue. As a result, the thickness of the bottom of the cushion is approximately 1 mm.

**Table 1.** Parameters of 3D printing a cushion made of TPU material, using the FDM method.

| Printer              |        | Print Settings |                    |                  | Speed       |           |          |
|----------------------|--------|----------------|--------------------|------------------|-------------|-----------|----------|
| Model                | Nozzle | Layer Height   | First Layer Height | Support Material | First Layer | Outskirts | Travel   |
| Artillery Sidewinder | 0.4 mm | 0.1 mm         | 0.2 mm             | no               | 20 mm/s     | 25 m/s    | 180 mm/s |

**Table 2.** Technical data of TPU material from the manufacturer—filament.

| Filament Manufacturer | Ø       | Color       | Shore Hardness | V-Notch Impact Strength | Young's Modulus | Density                |
|-----------------------|---------|-------------|----------------|-------------------------|-----------------|------------------------|
| PRINT-ME              | 1.75 mm | Fresh green | 20D            | 1.82 J/cm <sup>2</sup>  | 63 MPa          | 1.15 g/cm <sup>3</sup> |

### 2.2. Preliminary FEA

The magnetic field sources used in the investigation were a holding electromagnet with a diameter of 25 mm, height of 20 mm, and power supply parameters of 12 V 3.5 W (Figure 3a), and a magnetic holder of diameter 29 mm and height 8 mm having a magnet of diameter 24 mm and height 4 mm (Figure 3b). Figure 3 shows the result of a field source cushion simulation performed using the FEMM 4.2, a finite element method for electromagnetic solver. This software was provided by David Meeker, based on Lua 4.0 scripting engine [31]. For the purpose of the simulation, it is assumed that the entire volume of the cushion is filled with MRF-140CG magnetorheological fluid. The axisymmetric model was constrained by Dirichlet boundary conditions. Triangular mesh with smart option refining elements in vertices was used. Inner blocks have agglomerations with element size 0.8, vertices have elements with size 0.1. This approach provided meshes with a number of nodes in the range of 11,000 to 12,000, and number of elements approx. 23,000, depending on the geometry of the model. An example of a mesh is shown in Figure 3c. The

electromagnet is taken to be 3000 coil turns and 0.288 A supply current, which is observed in real conditions. The magnet material is N38. The cushion itself, made of TPU, has a magnetic permeability of a vacuum. A nonlinear characterization of the relationship of the magnetic flux density  $B$  (T) to the magnetic field strength  $H$  (A/m) of the MR fluid was implemented based on the manufacturer's documentation [32] and is shown in Figure 4, in accordance with Table 3.

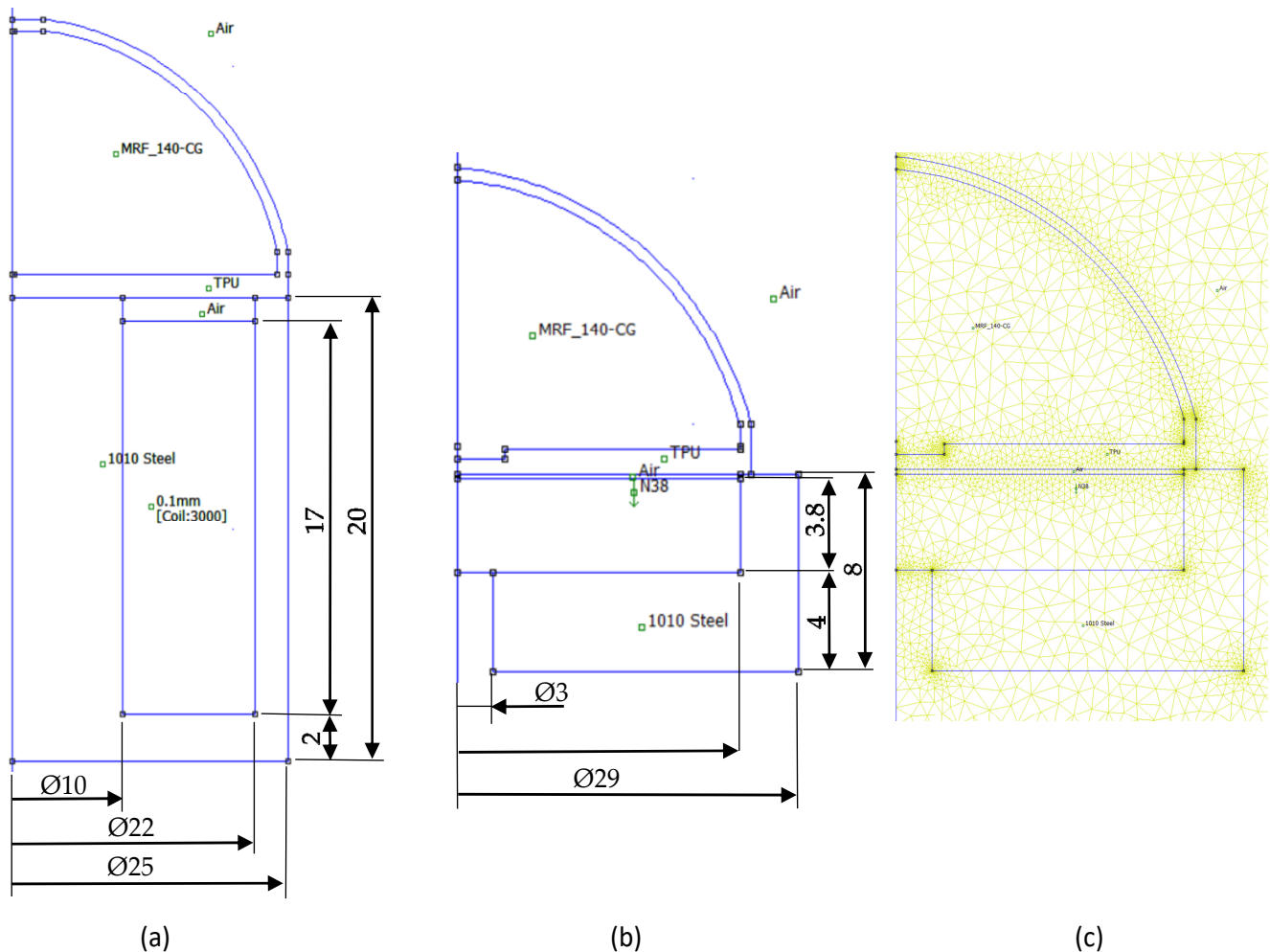


**Figure 3.** FE models of magnetic field exciters on the pin penetration setup; (a) cushion with electromagnet, (b) cushion with magnetic holder, (c) FE mesh for cushion with magnetic holder.

**Table 3.** Relationship between the magnetic flux density  $B$  (T) and the magnetic field strength  $H$  (kA/m) of the MRF-140CG [32].

| $B$ [T]    | 0.055 | 0.125 | 0.25 | 0.375 | 0.5 | 0.625 | 0.75  | 0.875 | 1     | 1.21 | 1.35 | 1.49 | 1.62 |
|------------|-------|-------|------|-------|-----|-------|-------|-------|-------|------|------|------|------|
| $H$ [kA/m] | 0     | 7.1   | 20.8 | 38.1  | 58  | 82.1  | 111.5 | 148.2 | 191.9 | 300  | 400  | 500  | 600  |

Comparative analysis of the determined magnetic flux density distributions in considered variants of the magnetic field excitation (shown in Figure 5) shows that in the case of the electromagnet excited system, the significant presence of the magnetic flux leakage can be observed (represented by the flux lines inside the coil area in Figure 5a not passing to the MR fluid container). In consequence, the magnetic flux density inside the cushion is relatively low and the magnetic field is not excited in the entire MR fluid volume. Moreover, the saturation of the yoke of the electromagnet can be observed.

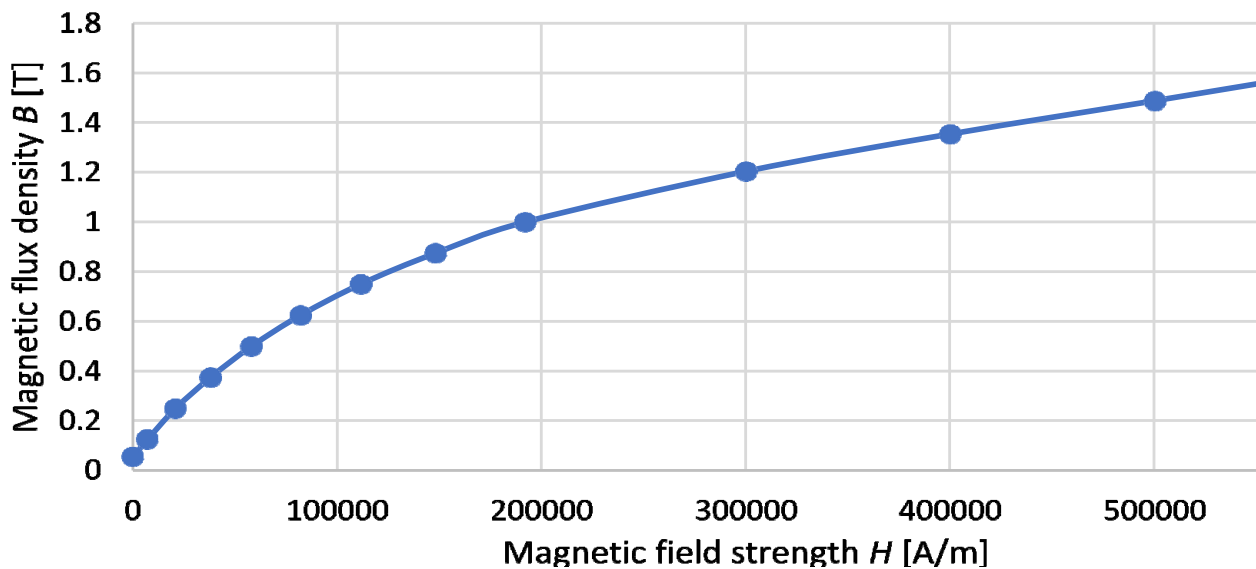


**Figure 4.** Nonlinear characterization of the relationship of the magnetic flux density  $B$  (T) to the magnetic field strength  $H$  (A/m) of the MRF-140CG [32].

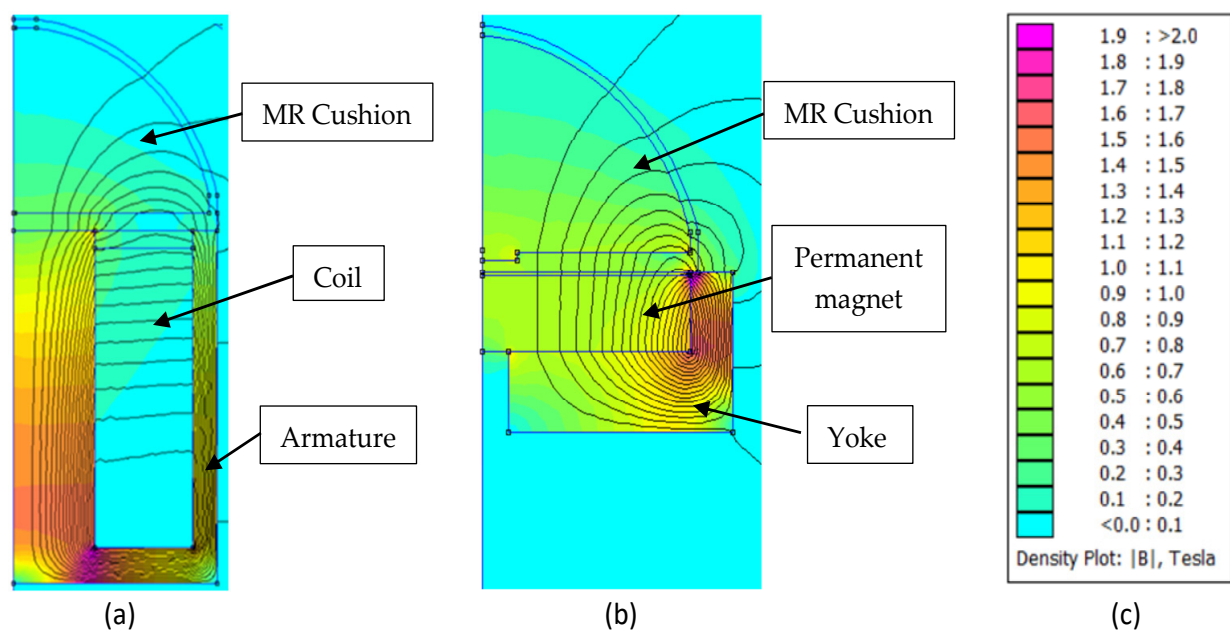


**Figure 5.** Determined magnetic flux density distributions in considered magnetic field exciters on the pin penetration setup; (a) cushion with electromagnet, (b) cushion with magnetic holder, (c) magnetic flux density scale.

The magnetic field distribution in the system excited by the permanent magnet holder is significantly different; the applied sintered neodymium iron boron (NdFeB) permanent magnet acts as strong magnetomotive source in the circuit. Despite the slightly saturated ferromagnetic yoke, it can be observed that the field source is strong enough to excite the magnetic field in the entire volume of the cushion.

It should be emphasized that conducted FEA deals only with the distribution of the magnetic field inside the considered system. In general, to study and compare the performance of the considered system in terms of impact on holding force of the gripper, the detailed and complex numerical model of the coupled phenomena should be developed. In such a model, besides the relation between the magnetic field and rheological properties of the MR fluid, the change of shape of cushion during the pin penetration should also be taken into account. Despite availability of the commercial and open-source tools for FEA

of different phenomena, such a problem, due to its complexity, has not been solved yet. On the other hand, it can be stated that the potential difference in performance of the studied systems will be related to the differences of the magnetic field distribution and may be evaluated by, and compared using, the experiment. Moreover, empirical comparison of the studied system's performance will allow one to assess the usefulness of the performed numerical models of the magnetic field in the system.

### 2.3. The Test Stand for the Investigations of a Pin Penetration into the Cushion

To evaluate the impact of the magnetic field distribution of the performance of the studied system, the cushions were tested on the developed test setup shown in Figure 6. It consists of a NA27 strain gauge beam (measuring range up to 20 N, repeatability  $\pm 0.03\%$  F.S.) with a mounted pin (diameter 7 mm), an HX711 amplifier with a measuring frequency of 80 Hz, a magnetic field source (in the form of an electromagnet and a permanent magnet—Figure 5), and a linear drive module with a screw. An Arduino Mega microcontroller development board was used to control the system and collect data. The procedure for conducting the measurement is shown in Figure 7.

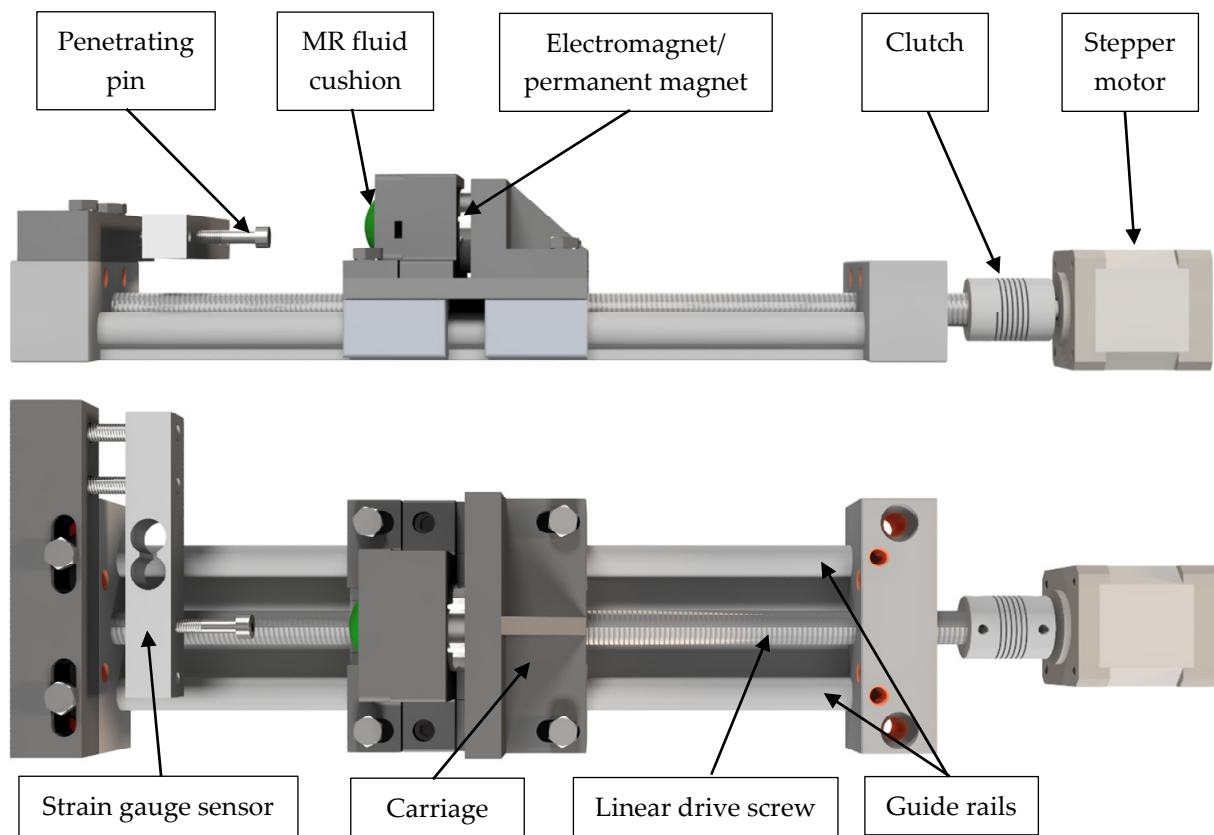


**Figure 6.** Construction of a test setup for penetrating the pin into the cushion.

The behavior of MR fluid is most commonly described by the Bingham plastic model. However, for the cushion under consideration, an additional modification in this model should be introduced. It requires the spring to be moved from the serial to parallel connection (Figure 7c). The total force generated by the cushion while pressing ( $\dot{x} > 0$ ) can be expressed by the formula

$$F(x) = F_s(x) + \text{sgn}(\dot{x})F_{MR}(B) + F_v(\dot{x}), \dot{x} > 0 \quad (1)$$

where  $F(x)$ —force changing in a function of displacement,  $F_s(x)$ —spring force generated by the compressed fluid and the cushion housing,  $F_v(\dot{x})$ —force resulting from plastic viscosity of the MR fluid, and  $F_{MR}(B)$ —force generated by the fluid being in magnetic field  $B$  while

pressing. This component describes the behavior of the MR fluid that turns into solid when minimum yield stress  $\tau_y(B)$  is achieved for magnetic flux density  $B \geq B_{min}$ . The spring force is the result of the geometrical deformation of the cushion housing, which is characterized by the stiffness of the TPU material with regard to its shape (especially thickness).

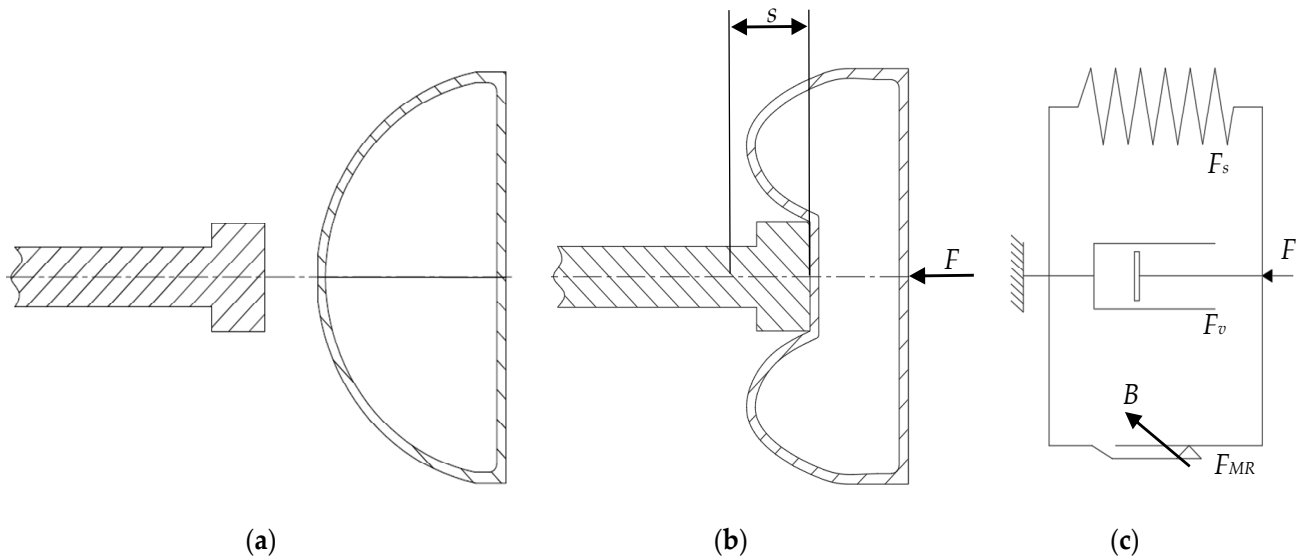


**Figure 7.** Illustration of the cushion deformation occurring as a result of the research carried out on the test setup shown in Figure 6; (a) the pin offset from the cushion, (b) the pin delves into the cushion as a result of the application of the force  $F$ —consequently, a hollow is observed with a depth of  $s$ , (c) mechanical model of the MR cushion.

### 3. Results

#### 3.1. Pin Penetration and Return Test Results

The test procedure is as follows. The pin attached to the strain gauge beam remains at rest. The cushion is in a holder, mounted on a carriage moving on a linear drive screw (Figure 6). During the first phase of movement, the cushion is positioned away from the pin and there is no contact between them (Figures 7a and 8a). The carriage, together with the cushion, begins to move in a uniform rectilinear motion. The starting point of the force–time plot in Figure 8 corresponds to the initiation of contact between the cushion face and the pin; this situation is illustrated in Figure 8b. The maximum penetration of the pin into the cushion is shown in Figures 7b and 8c. This state corresponds to the highest value of force recorded by the strain gauge beam observed in the force–time plot shown in Figure 8. At this point, there are two situations to be distinguished. The first, when the magnetic field is not introduced into the cushion (the waveform marked in blue), and the second, when the magnetic field is excited in the system (the waveform marked in orange). This allows to compare the effect of the field on the behavior of the MR fluid cushion. Figure 8d shows the effect of fixing the deformed shape of the cushion by the applied magnetic field. The recessed shape of the pin in the cushion is memorized, and pulling back the cushion shows the behavior of the imprinted pin shape. This can also be seen in the force–time plot, which illustrates a faster loss of contact and thus a reduction in the recorded load force. The situation shown in Figure 8e presents the absence of contact between the cushion and the pin in case of lack of a magnetic field. This is the end of the movement and measurement procedure.

**Table 4.** Cushion construction variants tested as part of the study.

|           | MR Fluid [mL] | Air [mL] | Void [mL] |
|-----------|---------------|----------|-----------|
| Variant 1 | 2.0           | 1.3      | 0         |
| Variant 2 | 2.0           | 0        | 1.3       |
| Variant 3 | 2.4           | 1.3      | 0         |
| Variant 4 | 2.4           | 0        | 1.3       |

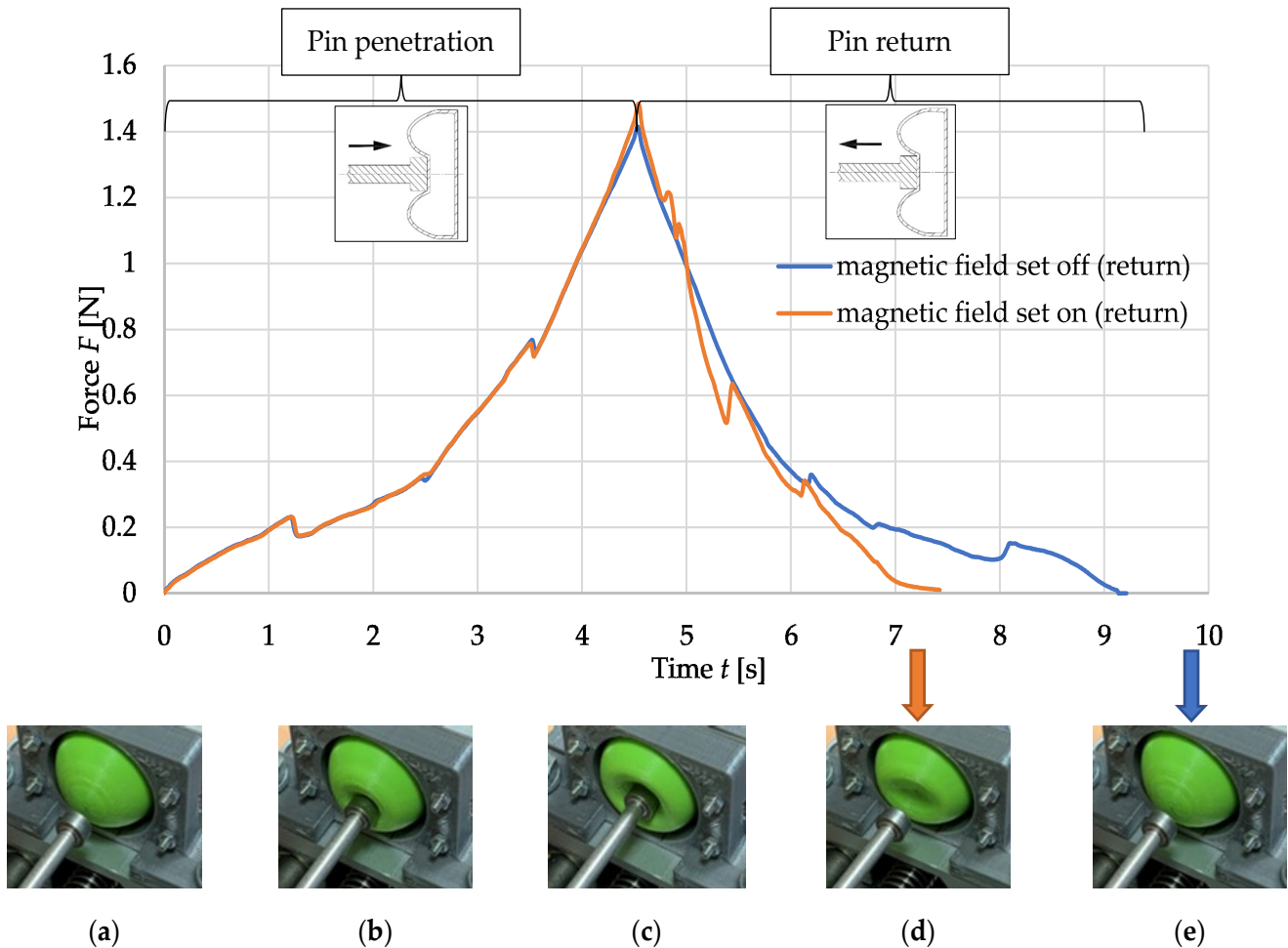


**Figure 8.** Test of denting the pin into a 2.0 mL cushion with unreleased air (Table 4: variant 1), force–time plot: (a) start of procedure—cushion is moving towards the pin; (b) establishing contact with the pin; (c) full penetration; (d) return phase—the cushion moves back from the pin; (e) loss of contact between cushion and pin.

The experiments were performed not only to examine the influence of the excitation type (electromagnet, magnetic holder) but also to study the impact of MR volume in the cushion, as well as the presence of the air inside the cushion. Considered variants of the MR fluid volume, as well as cushion construction, are summarized in Table 4. The volume of the inner cushion shell is approximately 3.3 mL. For the purpose of this study, two values of MR fluid insertion volume were provided: 2.0 mL (Table 4—variants 1 and 2) and 2.4 mL (Table 4—variants 3 and 4). Each of these volumes was furthermore performed in two configurations: with air retained inside when the cushion was closed (Table 4—variants 1 and 3), and air released creating a void (Table 4—variants 2 and 4). The first observations sighted the higher elasticity in compression of the cushions in which no air was released, and the concave shape of the cushions in which air was released.

For further analysis, the recorded force–time characteristics are plotted as a force function of displacement, corresponding to the penetration recess in the cushion (Figures 9 and 10).

The maximum pin recess  $s$  in the cushion reaches 8.5 mm (Figure 7b). The cushion behavior is not affected much by the electromagnet, as shown in Figure 9. The volume of fluid or the presence of air in the cushion is not relevant in this case. The following result of the experiment confirms the results of the preliminary FEA described in Section 2, which shows low magnetic flux density in the cushion volume (Figure 5a). Therefore, further analysis focuses on the use of the magnetic holder (Figure 5b).

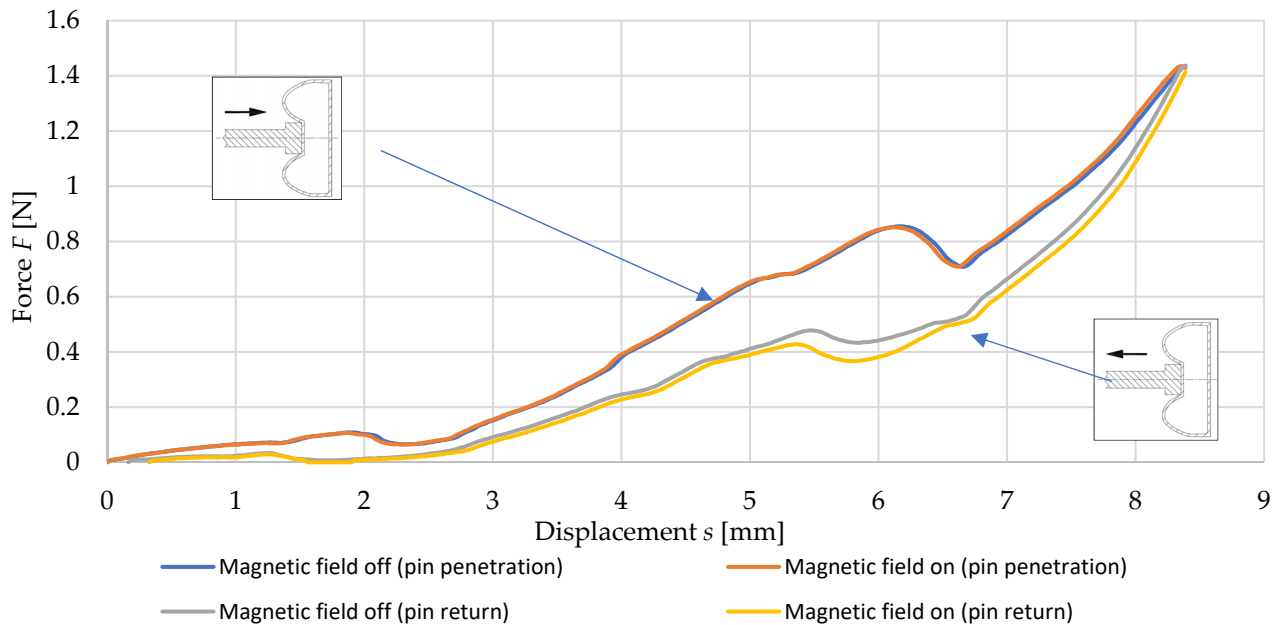


**Figure 9.** Force acting on the pin during penetration test for electromagnet and variant 2 cushion (Table 4), force–displacement characteristic.

The first significant difference is the higher elasticity of the cushions that had no air released (Figure 10a,c). The contact between the cushion face and the pin is retained for slightly longer compared to cushions in which air was released (Figure 10b,d). The presence of air results in a smoother fit when the cushion is retracted. The waveforms for these runs are smoother. It is also worth noting the difference between the return characteristics with the magnetic field present for the cushions with the air released. The larger volume of fluid also affects the elasticity of the cushion, as evidenced by the lack of a disruption when the pin is recessed in the characteristic in Figure 10d compared to Figure 10b. This fault is due to the deformation of the TPU cushion. For technological reasons of creating the cushion and ensuring its tightness, the dome is topped with a flattening piece (Figure 2a). When the pin is recessed, it is pressed into the center of the cushion. During this phase, due to the smaller fluid volume and the lack of air, there is a temporary reduction in force. The characteristics at retraction end at the same point, but it is smoother in Figure 10d compared to Figure 10b. Less fluid and displaced air also causes uneven deformation of the cushion. Consequently, the contact between the cushion and the pin is irregular and uneven while moving. The most accurate representation of the shape of the recessed pin was obtained for a 2.4 mL cushion with air released (Figure 10d). In this configuration, the cushion will behave more predictably regardless of the orientation in which it will operate. In addition, the air does not limit the movement of the MR fluid and the fit to the recessed shape. The presence of air can cause uneven fluid displacement, resulting in reduced stability of the grip and fluid distribution in the cushion volume.

Studying the comparison shown in Figure 11, particular attention should be paid to the distinctive rough characteristics of variant 2. The small volume of liquid and the released air result in a reduced elasticity of the cushion surface. For this reason, the surface of the cushion sphere is pulled raggedly away from the pin face during return. Note the

variant 4 with a larger volume of fluid, but also released air. The characteristics in this case are smoother, which is ensured by the elasticity of the liquid itself.

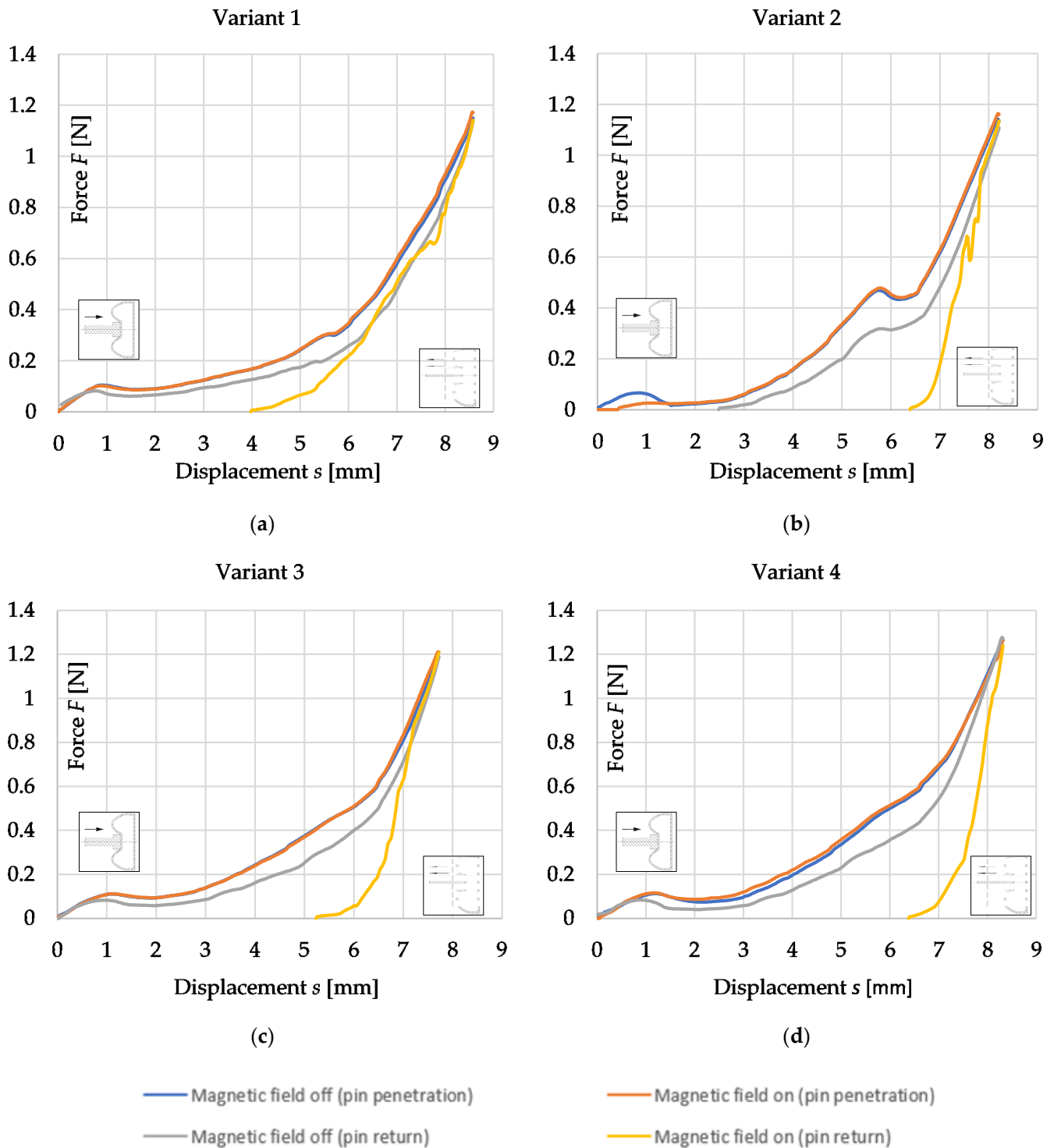


**Figure 10.** Force acting on the pin during penetration test for magnetic holder with respective variants of a cushion in accordance with Table 4, force–displacement characteristic. (a) Plot for 2.0 mL cushion with unreleased air—variant 1, (b) plot for 2.0 mL cushion with released air—variant 2, (c) plot for 2.4 mL cushion with unreleased air—variant 3, (d) plot for 2.4 mL cushion with released air—variant 4.

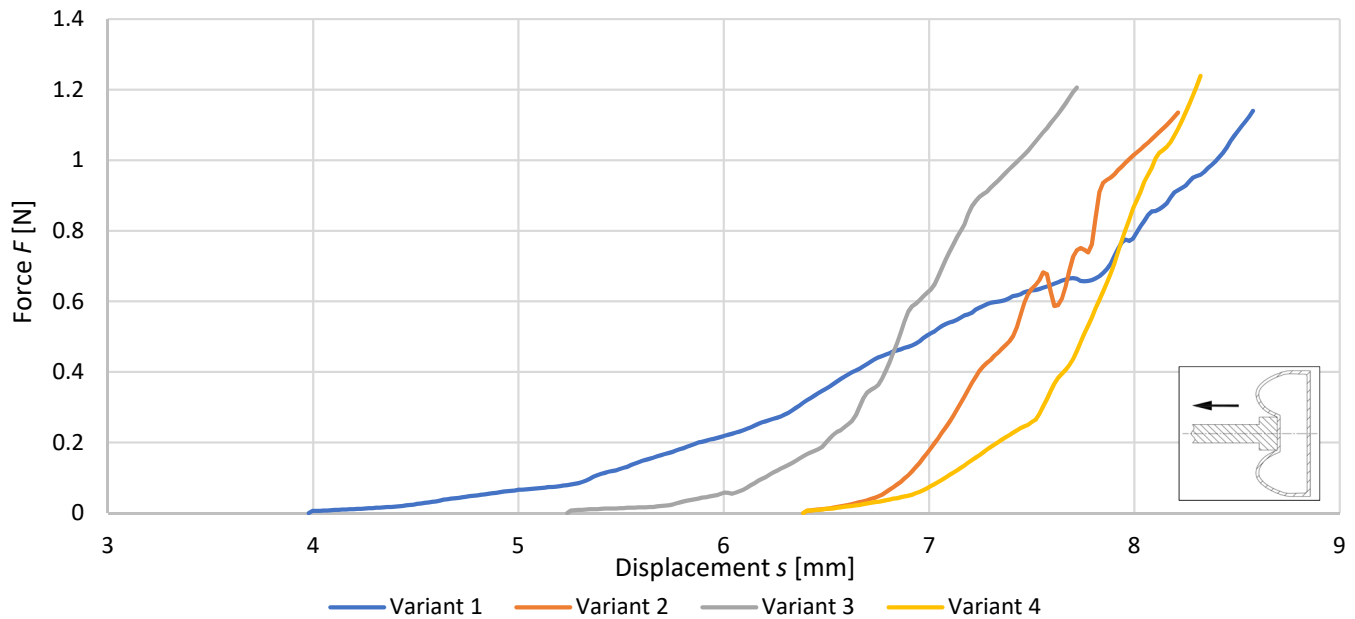


**Figure 11.** Comparison of the return phase for all cushion variants (in accordance with Table 4).

Based on analysis of results of the performed tests, further FEA studies of the magnetic field excitation system were conducted. The impact of the selected dimensions of the magnetic circuit on the magnetic field distribution inside the cushion were examined.

### 3.2. FEA of Magnetic Field Excitation System

Excluding the electromagnet as a source of magnetic field, the authors focused on developing a solution based on a permanent magnet. Taking into account the results of the tests to penetrate the pin into the cushion, it was therefore decided to carry out FEA of three magnetic holders of different sizes and shapes, denoted as model A (Figure 12a). Dimensions of permanent magnet of considered variants of model A are as follows: (a)  $\varnothing 29 \times 10$  mm, (b)  $\varnothing 20 \times 13$  mm, and (c)  $\varnothing 19 \times 8$  mm. The studied variants are based on shapes of the armature (see Figure 13a–c, respectively). The diameter of the variant denoted as (a) is larger than the cushion and, consequently, the armature, in which the magnet is located, protrudes beyond its outline (Figure 13a). The magnetic field lines coming out of the center of the magnet must pass through the MR fluid and the wall of the cushion to close. In the other two cases, the field is confined within the face of the cushion and does not extend beyond its walls. The holder in Figure 13b has a magnet with the same diameter as the holder in Figure 13c, except that it is 1 mm lower. Another key difference having impact on the magnetic field distribution between variants (b) and (c) is the geometry of the armature. The thicker armature on the bottom part of the magnetic circuit of variant (c) has a larger cross-sectional area, which is revealed by its lower saturation compared to the corresponding thinner armature of variant (b). On the other hand, all armatures have a common disadvantage, which is associated with the close proximity of the upper part of the yoke and the magnet. As it was mentioned when analyzing magnetic field distribution shown in Figure 5, the highest magnetic flux density can be observed at the border of the mentioned elements, i.e., between magnet edge and upper armature, at the bottom of the cushion. Thus, the field reaching the fluid inside at higher distances from the bottom of the cushion is relatively weak. To increase the magnetic field density at higher distances from the bottom of the cushion, an analysis of the application of the author's solution, considering of additional air gap between the magnet and a yoke, is needed.

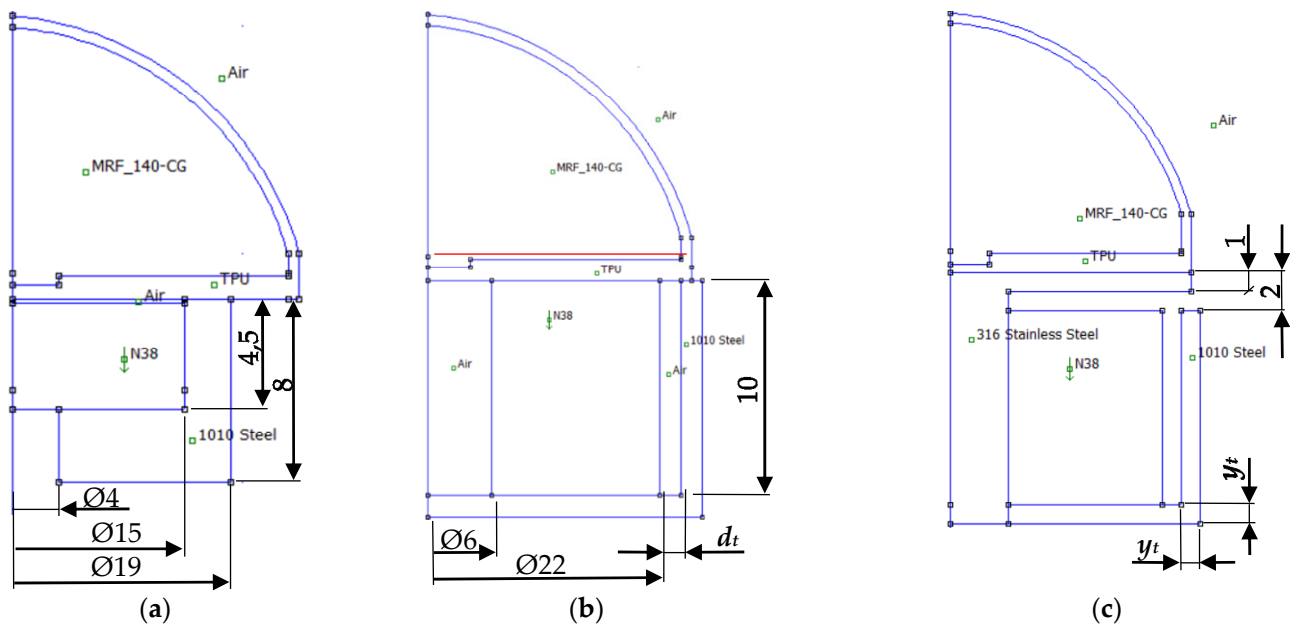


**Figure 12.** Models investigated using FEA; (a) model with magnetic holder, (b) model with permanent magnet and yoke, (c) model with permanent magnet, yoke, and pin in the core.

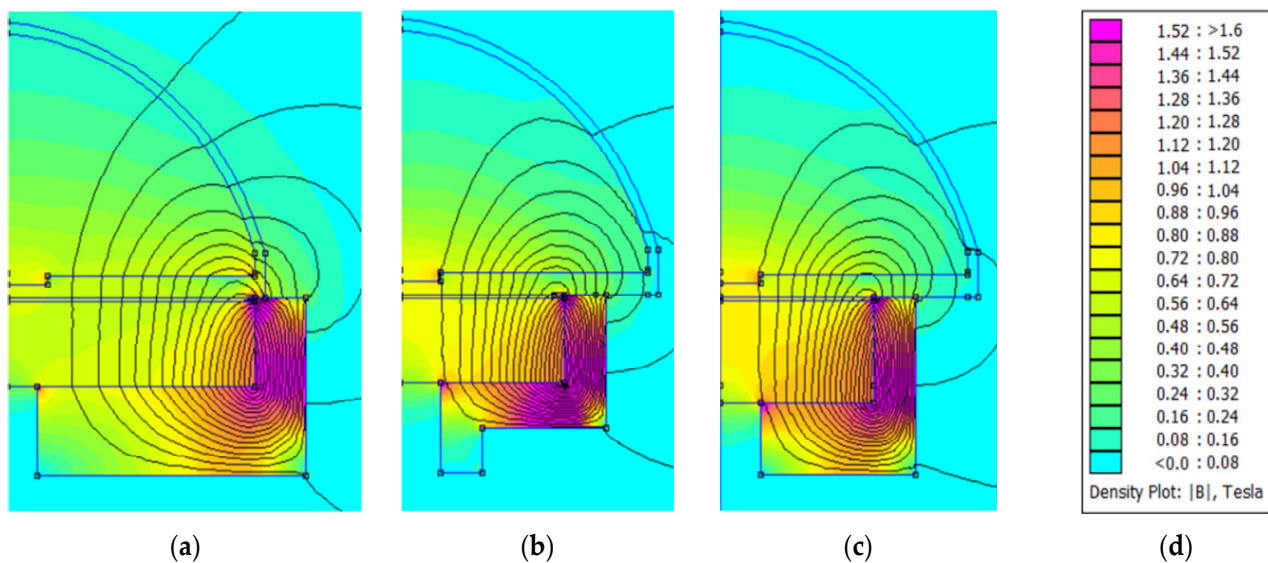


**Figure 13.** FEA results for model A; (a) magnetic mount fi29×10, (b) magnetic mount fi20×13, (c) magnetic mount fi19×8, (d) magnetic flux density scale in color representation.

Two author's solutions were prepared for further studies, denoted as model *B* (Figure 12b) and *C* (Figure 12c), respectively. Model *B* consists of an N38 permanent magnet (of 22 mm diameter and 10 mm height with a 6 mm diameter hole) placed inside the ferromagnetic yoke. The model *C* is an extension of model *B*, with an additional stainless pin placed inside the permanent magnet hole. For these cases, influence of two parameters was examined: the yoke thickness  $y_t$  of 0.5 and 1 mm and space between the yoke and the magnet  $d_t$  of 0, 0.5, 1, and 1.5 mm (as noted in Figure 12), respectively. The red line in Figure 12b indicates the test section, taken for analysis of the magnetic field density, located at a distance of 0.1 mm above the bottom of the cushion. The results of flux density in the cushion along the test line as a function of  $d_t$  for two values of  $y_t$  are shown in Figure 14a,c, respectively. The first thing worth noting, studying obtained results, is the higher flux density values for the thicker yoke (for instance 0.65 T for  $y_t = 0.5$  mm and 0.7T for

$y_t = 1$  mm at distance from the symmetry axis equal to 8 mm). Analogous to the magnetic holders discussed above, the increased yoke cross-section reduces the effect of saturation of the magnetic circuit. Nevertheless, the impact of  $d_t$  parameter on the magnetic flux density distribution for model B is not significant. Comparing the plots in Figure 14a,c it can be stated that slight differences occur close to the external border of the cushion (distance about 10 to 12 mm from the symmetry axis). In case of model B (see corresponding plots shown in Figure 15) for both yoke thicknesses, a clear effect of the  $d_t$  parameter is observed. However, studying the determined flux density plots, it can be stated that the impact of the additional air gap of values higher than 1 mm became insignificant. This can be observed especially in Figure 14c, as well as Figure 15a. It should also be taken into account that the analysis assumed a magnet with a fixed geometry in all considered variants. Increasing the  $d_t$  causes the yoke to extend beyond the outline of the cushion. This is illustrated in Figure 14b, showing the result of FEA for  $d_t = 1.0$  mm and  $y_t = 1.0$  mm. The effect of yoke thickness on the flux density distribution in the test plane is for model C is shown in Figure 15a,c. Analogue to results obtained for model B impact of yoke saturation is observed for  $y_t = 0.5$  mm. The flux density distribution along the test line for the 1.0 mm yoke is shifted upward in the flux density axis in relation to the 0.5 mm yoke.

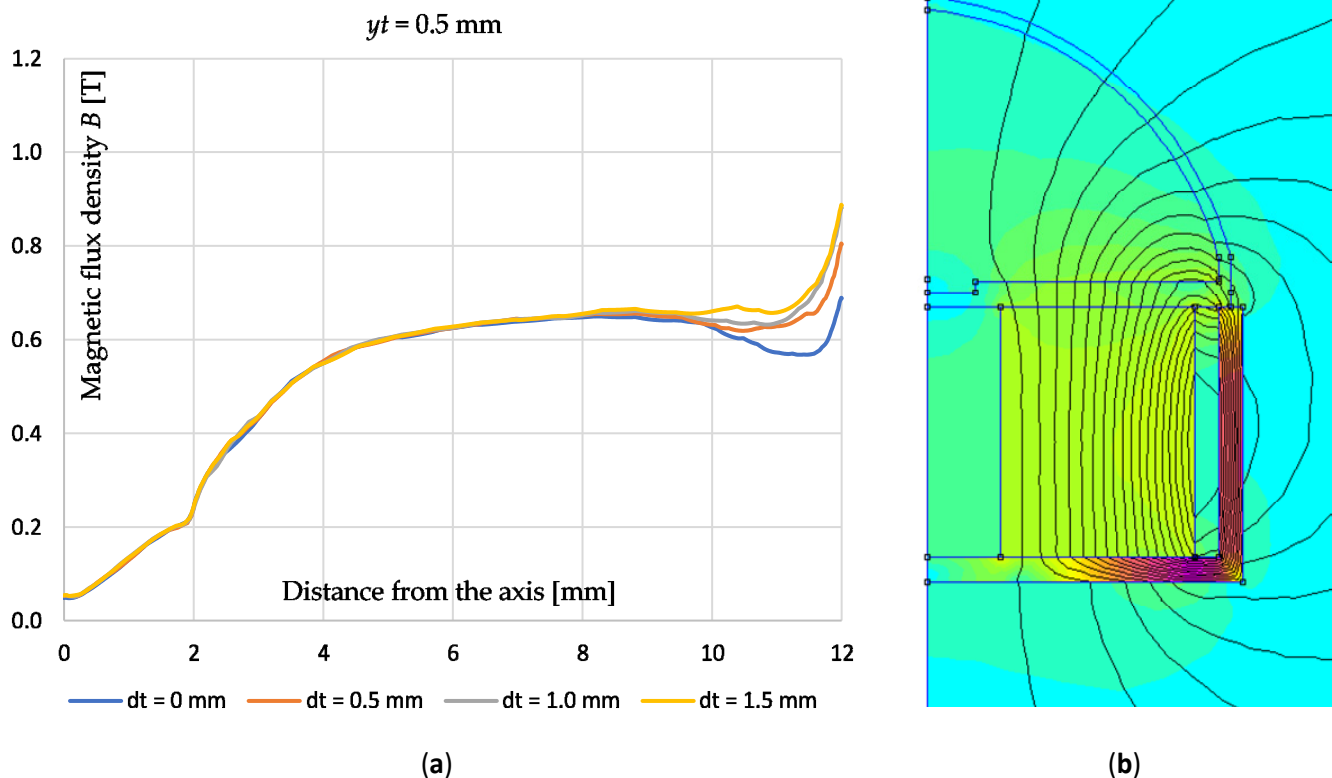
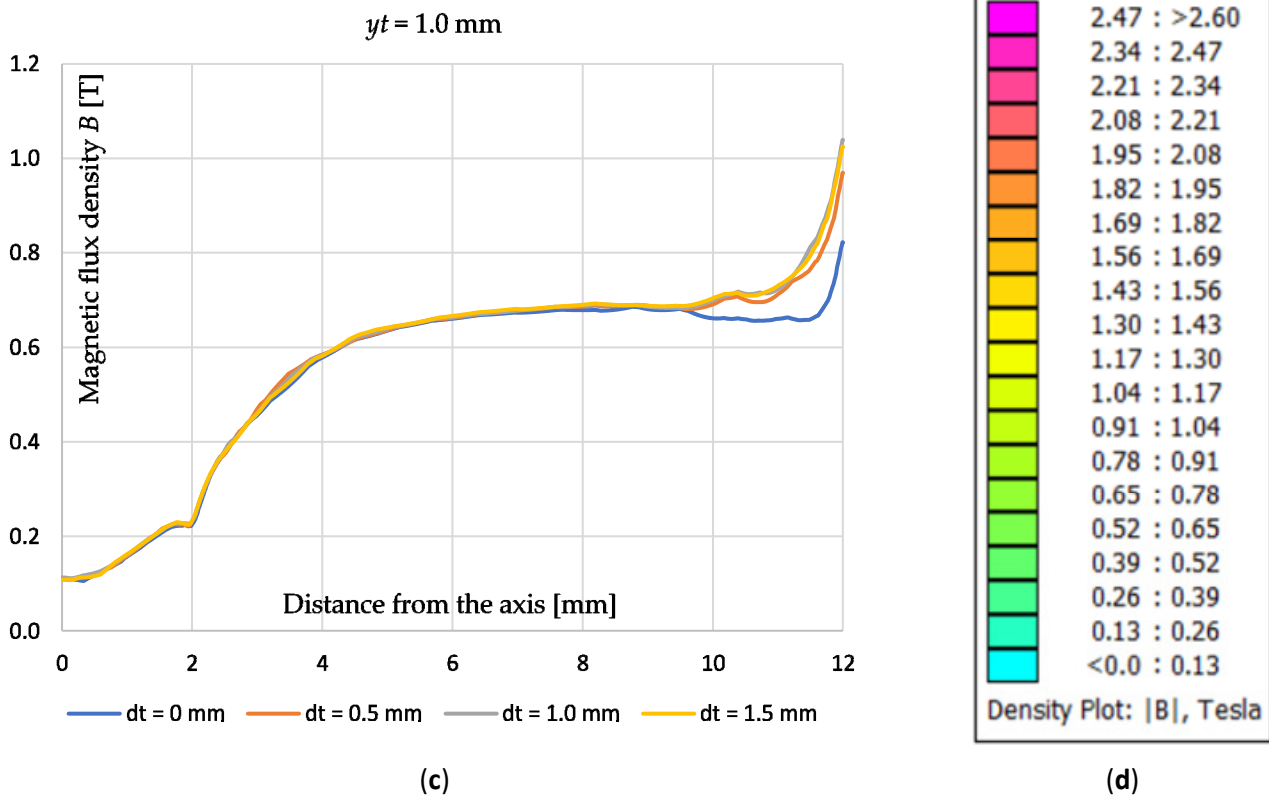
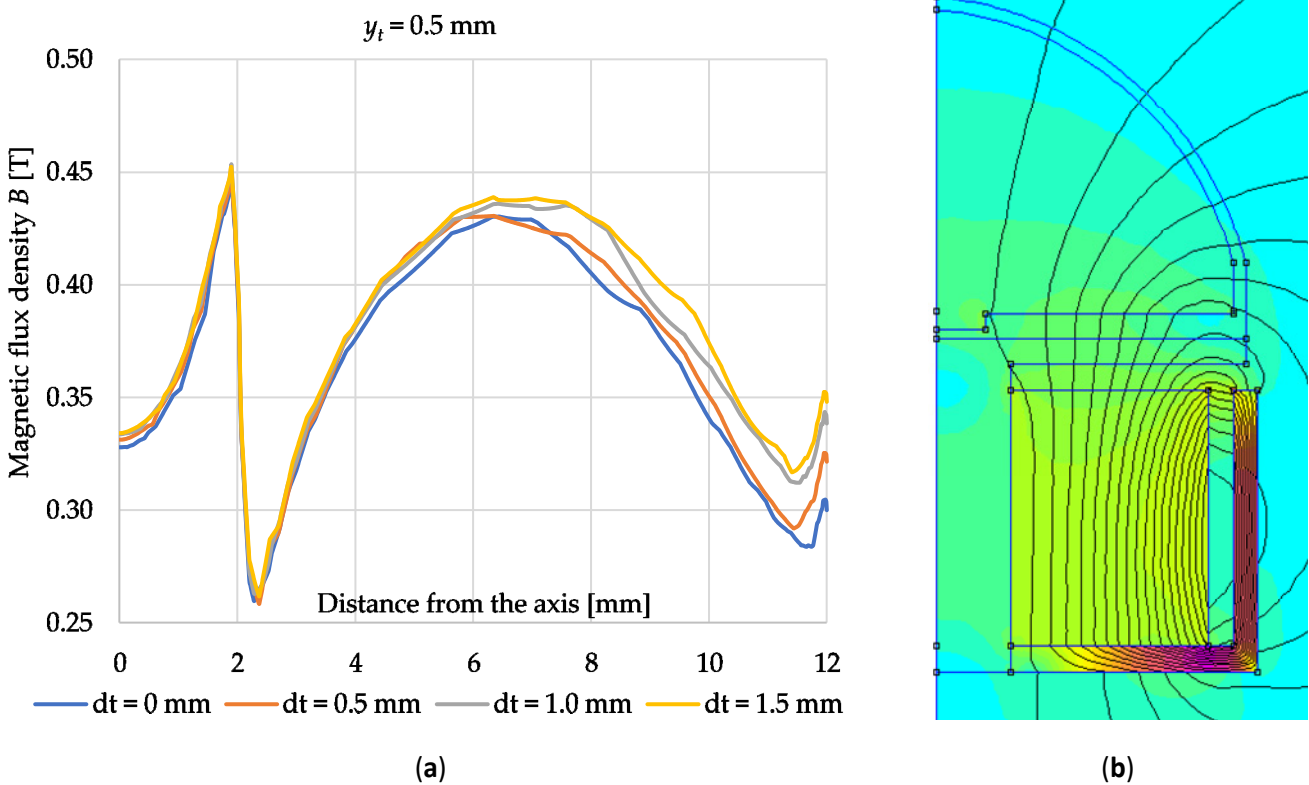


Figure 14. Cont.



**Figure 14.** FEA results for model B; (a) magnetic flux density characteristics as a function of distance from the axis in the plane 0.1 mm above the bottom of the cushion for  $y_t = 0.5 \text{ mm}$ , (b) magnetic flux density distribution for  $d_t = 1.0 \text{ mm}$  and  $y_t = 1.0 \text{ mm}$ , (c) magnetic flux density characteristics as a function of distance from the axis in the plane 0.1 mm above the bottom of the cushion for  $y_t = 1.0 \text{ mm}$ , (d) magnetic flux density scale in the color representation.



**Figure 15.** Cont.



inducing the MR fluid to organize its ferromagnetic particles along the field lines, is not met. The magnetic holder, by its compact design (no space between the magnet and the yoke), is not free from imperfections. The proximity of the yoke and magnet results in high saturation of the magnetic field flux density within the yoke, especially at the interface between the faces of the two elements. The subsequent pin penetration tests showed the uselessness of the electromagnet. The return characteristics (the offset of the pin from the cushion) are almost the same in this case with and without the magnetic field turned on. Promising results were obtained for the permanent magnet solution in the magnetic holder. Here, evidently, the presence of the magnetic field has a direct impact on the characteristics at pin return. As shown during the study, the volume of the MR fluid and the presence of air inside the cushion are also important. A potential field for further study would be the introduction of additional liquid volumes (the volume of the inner bowl is approximately 3.3 mL). However, preliminary tests showed that the introduction of too high a volume of MR liquid makes it difficult for the MR liquid to move inside the cushion, and thus prone to embedding objects. Therefore, it was decided to use volumes of 2.0 mL and 2.4 mL. The experimental results presented in this paper justify this decision.

Based on the analyses and measurements, two additional solutions based on magnets with holes were developed and analyzed. The studies were supplemented by further tests of the initially discussed magnetic holder in three size variants. They were subjected to FEA under the same conditions as presented earlier. This research was designed to indicate the potential impact of introducing a yoke with an air gap between the magnets. Model B is a precursor to the consideration of model C. The insertion of a pin in model C is necessary in order to place the cushion on a rigid support that will allow it to deform. Unfortunately, this also creates an additional barrier between the cushion and the magnetic field source. However, the results obtained are still satisfactory. The leading concept for target application of the soft-rigid gripper is the use of a spring to counteract the attraction force of the electromagnet, which will be developed in further stages of the work. This arrangement will allow the magnet to approach closer when the cushion is in contact with the gripping object in the gripper jaws. When the cushion jaws are moved apart, the distance between the magnet and the pillow will increase due to the spring reaction.

To determine the repeatability of the measurements, a comparative analysis of the overlap of readings from the strain gauge beam at the pin penetration section was adopted for 30 runs. For this purpose, the range of difference in sensor readings as a function of cushion displacement was determined. This resulted in an error of 1.66%, which is mainly due to the inaccuracy of the trapezoidal screw-based cushion drive set used.

Research focused on rheological properties of MR fluids shows that hysteresis of yield stress  $\tau_0$  against the change of the magnetic field density is marginal. Nevertheless, strong hysteresis of the transmitted torques or forces against excitation current can be observed in brakes or dampers with MR fluids [33,34]. Such behavior is caused by the impact of magnetic hysteresis of the ferromagnetic materials exploited in the magnetic circuit. In general, to reduce the effect of magnetic hysteresis on the performance of MR fluid transducers, the magnetic circuit should have a thin air gap in the main magnetic flux path. Presence of low permeability area acts as a load for the magnetic circuit and leads to demagnetization of the residual flux density. Residual magnetization leaves when the magnetizing field is removed. In the proposed system of magnetic field excitation, the cushion wall (made of paramagnetic TPU material) acts as a demagnetizing gap. Based on authors' experience dealing with numerical analysis of magnetic hysteresis in MR fluid devices [33], it is assumed that the impact of the magnetic hysteresis in studied magnetic circuits can be neglected. Validity of this assumption was confirmed by the fact that no impact of the magnetic hysteresis was observed in experimental results.

## 5. Conclusions

The research examined the potential of using an MR fluid in a cushion, along with its ability to change its viscosity by applying different magnetic field sources. Extensive

finite element analyses were carried out; simultaneously, the force acting on the pin during penetration tests of the cushion was examined. A TPU cushion material was successfully selected, and its geometry developed for 3D printing manufacturing technology.

The results are described in detail in the Discussion section and focus on research involving delving a pin into a cushion of small dimensions to demonstrate the ability to grasp objects by adapting to their shape. In addition, extensive FEA studies were carried out to identify potential ways of implementing a magnetic field source to stimulate the MR fluid within the cushion.

The study presented here provides a starting point for development in several directions that will be pursued by the authors. They helped to shape the perspective for the future work on the solution of the MR fluid cushion by recognizing the potential for selecting the source of the magnetic field and the dependent elements that affect its distribution within the cushion. Further research will include the ability to measure the pressures exerted on the cushion directly in its system, FE analysis of a cushion with a penetrated pin (optimization of magnet, yoke, and airspace dimensions), construction of a prototype based on a permanent magnet, yoke, and spring, as well as tests of the force acting in the plane perpendicular to the cushion's axis of rotation, and development and validation of proposed mathematical model.

## 6. Patents

The design solutions for the research results in this paper have been described in a patent application no. P.438636 filed in the Patent Office of the Republic of Poland.

**Author Contributions:** Conceptualization, M.B., C.J. and A.M.; methodology, M.B., C.J. and A.M.; software, M.B.; validation, M.B.; formal analysis, C.J.; investigation, M.B.; data curation, M.B.; writing—original draft preparation, M.B.; writing—review and editing, C.J. and A.M.; visualization, M.B.; supervision, C.J. All authors have read and agreed to the published version of the manuscript.

**Funding:** This research was supported by the National Ministry of Science and Higher Education in Poland as a part of research subsidy (project nos. 0614/SBAD/1529 and 0212/SBAD/0514).

**Institutional Review Board Statement:** Not applicable.

**Informed Consent Statement:** Not applicable.

**Data Availability Statement:** Not applicable.

**Conflicts of Interest:** The authors declare no conflict of interest.

## References

1. Terrile, S.; Argüelles, M.; Barrientos, A. Comparison of Different Technologies for Soft Robotics Grippers. *Sensors* **2021**, *21*, 3253. [[CrossRef](#)]
2. Cramer, J.; Cramer, M.; Demeester, E.; Kellens, K. Exploring the potential of magnetorheology in robotic grippers. *Procedia CIRP* **2018**, *76*, 127–132. [[CrossRef](#)]
3. Giannaccini, M.E.; Georgilas, I.; Horsfield, I.; Peiris, B.H.P.M.; Lenz, A.; Pipe, A.G.; Dogramadzi, S. A variable compliance, soft gripper. *Auton. Robot.* **2014**, *36*, 93–107. [[CrossRef](#)]
4. Homberg, B.S.; Katzschmann, R.K.; Dogar, M.R.; Rus, D. Haptic identification of objects using a modular soft robotic gripper. In Proceedings of the IEEE/RSJ International Conference on IROS, Hamburg, Germany, 28 September–2 October 2015; pp. 1698–1705. [[CrossRef](#)]
5. Calisti, M.; Arienti, A.; Renda, F.; Levy, G.; Hochner, B.; Mazzolai, B.; Dario, P.; Laschi, C. Design and development of a soft robot with crawling and grasping capabilities. In Proceedings of the IEEE International Conference on Robotics and Automation, Saint Paul, MN, USA, 14–18 May 2012; pp. 4950–4955. [[CrossRef](#)]
6. Hughes, J.; Culha, U.; Giardina, F.; Guenther, F.; Rosendo, A.; Iida, F. Soft Manipulators and Grippers: A Review. *Front. Robot. AI* **2016**, *3*, 1–12. [[CrossRef](#)]
7. Miron, G.; Bédard, B.; Plante, J.S. Sleeved Bending Actuators for Soft Grippers: A Durable Solution for High Force-to-Weight Applications. *Actuators* **2018**, *7*, 40. [[CrossRef](#)]
8. Park, W.; Seo, S.; Bae, J. A hybrid gripper with soft material and rigid structures. *IEEE Robot. Autom. Lett.* **2019**, *4*, 65–72. [[CrossRef](#)]

9. Cheng, P.; Jia, J.; Ye, Y.; Wu, C. Modeling of a Soft-Rigid Gripper Actuated by a Linear-Extension Soft Pneumatic Actuator. *Sensors* **2021**, *21*, 493. [CrossRef]
10. Cho, K.J.; Koh, J.S.; Kim, S.; Chu, W.S.; Hong, Y.; Ahn, S.H. Review of manufacturing processes for soft biomimetic robots. *Int. J. Precis. Eng. Manuf.* **2009**, *10*, 171–181. [CrossRef]
11. Cheng, N.G.; Gopinath, A.; Wang, L.; Iagnemma, K.; Hosoi, A.E. Thermally tunable, self-healing composites for soft robotic applications. *Macromol. Mater. Eng.* **2014**, *299*, 1279–1284. [CrossRef]
12. Camarillo, D.B.; Milne, C.F.; Carlson, C.R.; Zinn, M.R.; Salisbury, J.K. Mechanics modeling of tendon-driven continuum manipulators. *IEEE Trans. Robot.* **2008**, *24*, 1262–1273. [CrossRef]
13. Camarillo, D.B.; Carlson, C.R.; Salisbury, J.K. Configuration tracking for continuum manipulators with coupled tendon drive. *IEEE Trans. Robot.* **2009**, *25*, 798–808. [CrossRef]
14. Amend, J.R.; Brown, E.; Rodenberg, N.; Jaeger, H.M.; Lipson, H. A positive pressure universal gripper based on the jamming of granular material. *IEEE Trans. Robot.* **2012**, *28*, 341–350. [CrossRef]
15. Nishida, T.; Okatani, Y.; Tadakuma, K. Development of universal robot gripper using mr  $\alpha$  fluid. *Int. J. Hum. Robot.* **2016**, *13*, 1–13. [CrossRef]
16. Choi, Y.T.; Hartzell, C.M.; Leps, T.; Wereley, N.M. Gripping characteristics of an electromagnetically activated magnetorheological fluid-based gripper. *AIP Adv.* **2018**, *8*, 1–6. [CrossRef]
17. Hartzell, C.M.; Choi, Y.T.; Wereley, N.M.; Leps, T.J. Performance of a magnetorheological fluid-based robotic end effector. *Smart Mater. Struct.* **2019**, *28*, 1–8. [CrossRef]
18. Tsugami, Y.; Nishida, T. Simple structured gripper using electromagnet and permanent magnet. In Proceedings of the International Conference on ICT Robotics, Kagoshima, Japan, 25–26 November 2017; pp. 64–67.
19. Maruyama, R.; Watanabe, T.; Uchida, M. Delicate grasping by robotic gripper with incompressible fluid-based deformable fingertips. In Proceedings of the IEEE/RSJ International Conference on Intelligent Robots and Systems, Tokyo, Japan, 3–7 November 2013; pp. 5469–5474. [CrossRef]
20. Nishimura, T.; Suzuki, Y.; Tsuji, T.; Watanabe, T. Fluid pressure monitoring-based strategy for delicate grasping of fragile objects by a robotic hand with fluid fingertips. *Sensors* **2019**, *19*, 782. [CrossRef]
21. Choi, H.; Koc, M. Design and feasibility tests of a flexible gripper based on inflatable rubber pockets. *Int. J. Mach. Tools Manuf.* **2006**, *46*, 1350–1361. [CrossRef]
22. Tsugami, Y.; Barbié, T.; Tadakuma, K.; Nishida, T. Development of Universal Parallel Gripper Using Reformed Magnetorheological Fluid. In Proceedings of the 11th Asian control conference (ASCC) IEEE, Gold Coast, Australia, 17–20 December 2017; pp. 778–783. [CrossRef]
23. Leddy, M.T.; Dollar, A.M. Examining the frictional behavior of primitive contact geometries for use as robotic finger pads. *IEEE Robot. Autom. Lett.* **2020**, *5*, 3137–3144. [CrossRef]
24. Spiers, A.J.; Calli, B.; Dollar, A.M. Variable-friction finger surfaces to enable within-hand manipulation via gripping and sliding. *IEEE Robot. Autom. Lett.* **2018**, *3*, 4116–4123. [CrossRef]
25. Costanzo, M.; De Maria, G.; Natale, C. Two-fingered in-hand object handling based on force/tactile feedback. *IEEE Trans. Robot.* **2019**, *36*, 157–173. [CrossRef]
26. Białek, M.; Rybarczyk, D.; Milecki, A.; Nowak, P. Artificial hand controlled by a glove with a force feedback. In *Advances in Manufacturing II*; Volume 1—Solutions for Industry 4.0; Springer: Berlin/Heidelberg, Germany, 2019; pp. 444–455. [CrossRef]
27. Rybarczyk, D.; Owczarek, P.; Myszkowski, A. Development of Force Feedback Controller For the Loader Crane. In *Advances in Manufacturing—Lecture Notes in Mechanical Engineering*; Springer: Berlin/Heidelberg, Germany, 2018; pp. 345–354. [CrossRef]
28. Oh, J.-S.; Sohn, J.W.; Choi, S.-B. Material Characterization of Hardening Soft Sponge Featuring MR Fluid and Application of 6-DOF MR Haptic Master for Robot-Assisted Surgery. *Materials* **2018**, *11*, 1268. [CrossRef] [PubMed]
29. Naimzad, A.; Ghodsi, M.; Hojjat, Y.; Maddah, A. MREs development and its application on miniature gripper. In Proceedings of the International Conference on Advanced Materials Engineering, Suntec, Singapore, 26 June–1 July 2011; Volume 15, pp. 75–79.
30. Zhou, J.; Chen, S.; Wang, Z. A soft-robotic gripper with enhanced object adaptation and grasping reliability. *IEEE Robot. Autom. Lett.* **2017**, *2*, 2287–2293. [CrossRef]
31. Finite Element Method Magnetics by David Meeker. Available online: <https://www.femm.info/wiki/HomePage> (accessed on 18 March 2021).
32. LORD MR Fluid Manufacturer. Available online: [https://lordfulfillment.com/pdf/44/DS7012\\_MRF-140CGMRFluid.pdf](https://lordfulfillment.com/pdf/44/DS7012_MRF-140CGMRFluid.pdf) (accessed on 11 October 2021).
33. Jędrzycka, C.; Sujka, P.; Szela, W. The influence of magnetic hysteresis on magnetorheological fluid clutch operation. *COMPEL-Int. J. Comput. Math. Electr. Electron. Eng.* **2009**, *28*, 711–721. [CrossRef]
34. Guan, X.C.; Guo, P.F.; Ou, J.P. Modeling and analyzing of hysteresis behavior of magneto rheological dampers. *Procedia Eng.* **2011**, *14*, 2756–2764. [CrossRef]